Field enhancement in metallic subwavelength aperture arrays probed by erbium upconversion luminescence

Ewold Verhagen, L. Kuipers, and Albert Polman

Center for Nanophotonics, FOM-Institute for Atomic and Molecular Physics (AMOLF), Science Park 113, 1098 XG Amsterdam, The Netherlands

verhagen@amolf.nl

Abstract: Upconversion luminescence from erbium ions placed in the near field of subwavelength aperture arrays is used to investigate field enhancement of incident near-infrared light in such nanostructures. We study field enhancement due to the excitation of both propagating and localized surface plasmon resonances in arrays of square and annular apertures in a Au film. The conversion of 1480 nm excitation light to 980 nm emission is shown to be enhanced up to a factor 450 through a subwavelength hole array. The effects of array periodicity and aperture size are investigated. It is shown that a Fano model can describe both far-field transmission and near-field intensity. The upconversion enhancement reveals the wavelength and linewidth of the surface plasmon modes that are responsible for extraordinary transmission in such arrays. Angle-dependent measurements on annular aperture arrays prove that the field enhancement due to localized resonances is independent of the incident angle. These experiments provide insight in the mechanisms responsible for extraordinary transmission and are important for applications that aim to exploit near-field enhancement in nanostructured metal films.

OCIS codes: (240.6680) Optics at surfaces: surface plasmons ; (050.6624) Diffraction and gratings: apertures ; (300.1220) Spectroscopy ; fluorescence, laser-induced.

References and links

1. T. W. Ebbesen, H. J. Lezec, H. F. Ghaemi, T. Thio, and P. A. Wolff, "Extraordinary optical transmission through sub-wavelength hole arrays," Nature **391**(6668), 667–669 (1998).
2. C. Genet and T. W. Ebbesen, "Light in tiny holes," Nature **445**(7123), 39–46 (2007).
3. F. J. García de Abajo, "Colloquium: Light scattering by particle and hole arrays," Rev. Mod. Phys. **79**(4) (2007).
4. A. G. Brolo, E. Arctander, R. Gordon, B. Leathem, and K. L. Kavanagh, "Nanohole-Enhanced Raman Scattering," Nano Lett. **4**(10), 2015–2018 (2004).
5. M. Tanaka, F. Miyamaru, M. Hangyo, T. Tanaka, M. Akazawa, and E. Sano, "Effect of a thin dielectric layer on terahertz transmission characteristics for metal hole arrays," Opt. Lett. **30**(10), 1210–1212 (2005).
6. Y. Liu and S. Blair, "Fluorescence enhancement from an array of subwavelength metal apertures," Opt. Lett. **28**(7), 507–509 (2003).
7. A. G. Brolo, S. C. Kwok, M. D. Cooper, M. G. Moffitt, C.-W. Wang, R. Gordon, J. Riordon, and K. L. Kavanagh, "Surface Plasmon-Quantum Dot Coupling from Arrays of Nanoholes," J. Phys. Chem. B **110**(16), 8307–8313 (2006).
8. M. Airola, Y. Liu, and S. Blair, "Second-harmonic generation from an array of sub-wavelength metal apertures," J. Opt. A: Pure Appl. Opt. **7**(2), S118–S123 (2005).
9. J. A. H. van Nieuwstadt, M. Sandtke, R. H. Harmsen, F. B. Segerink, J. C. Prangsma, S. Enoch, and L. Kuipers, "Strong Modification of the Nonlinear Optical Response of Metallic Subwavelength Hole Arrays," Phys. Rev. Lett. **97**(14), 146102 (2006).

#113798 - $15.00 USD Received 6 Jul 2009; revised 29 Jul 2009; accepted 30 Jul 2009; published 3 Aug 2009

10. W. Fan, S. Zhang, N.-C. Panoiu, A. Abdenour, S. Krishna, R. M. Osgood, K. J. Malloy, and S. R. J. Brueck, "Second Harmonic Generation from a Nanopatterned Isotropic Nonlinear Material," Nano Lett. **6**(5), 1027–1030 (2006).
11. W. Fan, S. Zhang, K. J. Malloy, S. R. J. Brueck, N. C. Panoiu, and R. M. Osgood, "Second harmonic generation from patterned GaAs inside a subwavelength metallic hole array," Opt. Express **14**(21), 9570–9575 (2006).
12. P. Lalanne, J. C. Rodier, and J. P. Hugonin, "Surface plasmons of metallic surfaces perforated by nanohole arrays," J. Opt. A: Pure Appl. Opt. **7**(8), 422–426 (2005).
13. K. J. Klein Koerkamp, S. Enoch, F. B. Segerink, N. F. van Hulst, and L. Kuipers, "Strong Influence of Hole Shape on Extraordinary Transmission through Periodic Arrays of Subwavelength Holes," Phys. Rev. Lett. **92**(18), 183901 (2004).
14. F. J. García-Vidal, E. Moreno, J. A. Porto, and L. Martín-Moreno, "Transmission of Light through a Single Rectangular Hole," Phys. Rev. Lett. **95**(10), 103901 (2005).
15. F. I. Baida and D. Van Labeke, "Light transmission by subwavelength annular aperture arrays in metallic films," Opt. Commun. **209**, 17–22 (2002).
16. F. I. Baida and D. Van Labeke, "Three-dimensional structures for enhanced transmission through a metallic film: Annular aperture arrays," Phys. Rev. B **67**(15), 155314 (2003).
17. W. Fan, S. Zhang, B. Minhas, K. J. Malloy, and S. R. J. Brueck, "Enhanced Infrared Transmission through Subwavelength Coaxial Metallic Arrays," Phys. Rev. Lett. **94**(3), 033902 (2005).
18. F. Baida, D. Van Labeke, G. Granet, A. Moreau, and A. Belkhir, "Origin of the super-enhanced light transmission through a 2-D metallic annular aperture array: a study of photonic bands," Appl. Phys. B: Lasers Opt. **79**(1), 1–8 (2004).
19. S. M. Orbons and A. Roberts, "Resonance and extraordinary transmission in annular aperture arrays," Opt. Express **14**(26), 12623–12628 (2006).
20. F. I. Baida, A. Belkhir, D. Van Labeke, and O. Lamrous, "Subwavelength metallic coaxial waveguides in the optical range: Role of the plasmonic modes," Phys. Rev. B **74**(20) (2006).
21. M. I. Haftel, C. Schlockermann, and G. Blumberg, "Enhanced transmission with coaxial nanoapertures: Role of cylindrical surface plasmons," Phys. Rev. B **74**(23) (2006).
22. D. Van Labeke, D. Gérard, B. Guizal, F. I. Baida, and L. Li, "An angle-independent Frequency Selective Surface in the optical range," Opt. Express **14**(25), 11945–11951 (2006).
23. F. Auzel, "Upconversion and Anti-Stokes Processes with f and d Ions in Solids," Chem. Rev. **104**(1), 139–174 (2004).
24. G. N. van den Hoven, E. Snoeks, A. Polman, C. van Dam, J. W. M. van Uffelen, and M. K. Smit, "Upconversion in Er-implanted Al_2O_3 waveguides," J. Appl. Phys. **79**(3), 1258–1266 (1996).
25. W. von Klitzing, E. Jahier, R. Long, F. Lissillour, V. Lefevre-Seguin, J. Hare, J.-M. Raimond, and S. Haroche, "Very low threshold green lasing in microspheres by up-conversion of IR photons," J. Opt. B: Quantum Semiclassical Opt. **2**(2), 204–206 (2000).
26. E. Heumann, S. Bär, K. Rademaker, G. Huber, S. Butterworth, A. Diening, and W. Seelert, "Semiconductor-laser-pumped high-power upconversion laser," Appl. Phys. Lett. **88**(6) (2006).
27. T. Lu, L. Yang, R. V. A. van Loon, A. Polman, and K. J. Vahala, "On-chip green silica upconversion microlaser," Opt. Lett. **34**(4), 482–484 (2009).
28. E. Downing, L. Hesselink, J. Ralston, and R. Macfarlane, "A Three-Color, Solid-State, Three-Dimensional Display," Science **273**(5279), 1185–1189 (1996).
29. S. F. Lim, R. Riehn, W. S. Ryu, N. Khanarian, C.-k. Tung, D. Tank, and R. H. Austin, "In Vivo and Scanning Electron Microscopy Imaging of Upconverting Nanophosphors in Caenorhabditis elegans," Nano Lett. **6**(2), 169–174 (2006).
30. T. Trupke, M. A. Green, and P. Würfel, "Improving solar cell efficiencies by up-conversion of sub-band-gap light," J. Appl. Phys. **92**(7), 4117–4122 (2002).
31. F. Hallermann, C. Rockstuhl, S. Fahr, G. Seifert, S. Wackerow, H. Graener, G. v. Plessen, and F. Lederer, "On the use of localized plasmon polaritons in solar cells," Phys. Status Solidi A **205**(12), 2844–2861 (2008).
32. S. Baluschev, F. Yu, T. Miteva, S. Ahl, A. Yasuda, G. Nelles, W. Knoll, and G. Wegner, "Metal-Enhanced Up-Conversion Fluorescence: Effective Triplet-Triplet Annihilation near Silver Surface," Nano Lett. **5**(12), 2482–2484 (2005).
33. T. Aisaka, M. Fujii, and S. Hayashi, "Enhancement of upconversion luminescence of Er doped Al_2O_3v films by Ag island films," Appl. Phys. Lett. **92**(13) (2008).
34. V. K. Rai, L. de S. Menezes, C. B. de Araújo, L. R. P. Kassab, D. M. da Silva, and R. A. Kobayashi, "Surface-plasmon-enhanced frequency upconversion in Pr^{3+} doped tellurium-oxide glasses containing silver nanoparticles," J. Appl. Phys. **103**(9) (2008).
35. URL: www.srim.org.
36. G. N. van den Hoven, E. Snoeks, A. Polman, J. W. M. van Uffelen, Y. S. Oei, and M. K. Smit, "Photoluminescence characterization of Er-implanted Al_2O_3 films," Appl. Phys. Lett. **62**(24), 3065–3067 (1993).
37. A. Moreau, G. Granet, F. Baida, and D. V. Labeke, "Light transmission by subwavelength square coaxial aperture arrays in metallic films," Opt. Express **11**(10), 1131–1136 (2003).

#113798 - $15.00 USD Received 6 Jul 2009; revised 29 Jul 2009; accepted 30 Jul 2009; published 3 Aug 2009

38. J. Kalkman, L. Kuipers, A. Polman, and H. Gersen, "Coupling of Er ions to surface plasmons on Ag," Appl. Phys. Lett. **86**, 041113 (2005).
39. H. F. Ghaemi, T. Thio, D. E. Grupp, T. W. Ebbesen, and H. J. Lezec, "Surface plasmons enhance optical transmission through subwavelength holes," Phys. Rev. B **58**, 6779 (1998).
40. W. L. Barnes, W. A. Murray, J. Dintinger, E. Devaux, and T. W. Ebbesen, "Surface plasmon polaritons and their role in the enhanced transmission of light through periodic arrays of subwavelength holes in a metal film," Phys. Rev. Lett. **92**, 107401 (2004).
41. K. L. van der Molen, F. B. Segerink, N. F. van Hulst, and L. Kuipers, "Influence of hole size on the extraordinary transmission through subwavelength hole arrays," Appl. Phys. Lett. **85**(19), 4316–4318 (2004).
42. U. Fano, "Effects of Configuration Interaction on Intensities and Phase Shifts," Phys. Rev. **124**(6), 1866–1878 (1961).
43. M. Sarrazin, J.-P. Vigneron, and J.-M. Vigoureux, "Role of Wood anomalies in optical properties of thin metallic films with a bidimensional array of subwavelength holes," Phys. Rev. B **67**(8), 085415 (2003).
44. C. Genet, M. P. van Exter, and J. P. Woerdman, "Fano-type interpretation of red shifts and red tails in hole array transmission spectra," Opt. Commun. **225**, 331 – 336 (2003).
45. H. A. Bethe, "Theory of Diffraction by Small Holes," Phys. Rev. **66**(7-8), 163–182 (1944).

1. Introduction

There has been a large interest in subwavelength aperture arrays in metallic films ever since the first report of extraordinary transmission through such structures [1]. Much effort has been dedicated to elucidating the fundamental principles that govern the far-field properties of aperture arrays [2, 3]. Additionally, the enhancement of the near field in aperture arrays due to the excitation of optical resonances has been recognized to yield many possible applications. Among those applications are efficient sensing [4, 5], strong control over light extraction [6, 7] and the enhancement of nonlinear effects [8–11]. Broadly speaking, two types of resonances can be distinguished that are responsible for the main transmission peaks observed in far-field transmission spectra as well as for the accompanying enhancement of the near field. The first type relies on the resonant excitation of surface waves (surface plasmon polaritons (SPPs) for optical frequencies) propagating along the metal film surface. As the excitation is due to grating diffraction, this effect depends strongly on incident angle and wavelength. The responsible surface waves can be described as eigenmodes of the corrugated metal surface [12]. Secondly, properly shaped apertures can support localized plasmonic modes that can lead to very large transmission [13, 14]. In particular, arrays of annular apertures exhibit a strong transmission resonance [15–17]. This resonance is associated to the cutoff condition for the TE_{11} mode propagating inside individual apertures [18–21]. A single aperture can be viewed as a truncated waveguide. Bounded by the air and substrate outside the metal film, it forms a low quality factor optical cavity. At cutoff, the wavevector of the TE_{11} mode propagating inside this waveguide approaches zero, which results in a cavity resonance that is independent of the metal film thickness. Because of the localized nature of the mode, this transmission resonance is independent of incident angle and polarization [22], which is a large benefit for many applications. Moreover, the resonance has a wide bandwidth.

In this work, we investigate field enhancement in aperture arrays supporting both types of resonances using the photoluminescence from emitters placed in the near field of the metallic nanostructures. The emitters are erbium ions located in the sapphire substrate at an average depth of 35 nm below the structured Au film. The Er ions can convert infrared radiation with a free-space wavelength of 1480 nm to emission at shorter wavelengths (most notably at 980 nm) through an upconversion process [23, 24]. The upconversion luminescence emitted into the far field is used as a direct probe of the local field intensity at the position of the Er ions. We find that the emitted upconversion luminescence from Er ions excited through hole arrays supporting propagating surface plasmon resonances can be enhanced up to a factor of 450. We investigate the influence of hole size and array periodicity on the field enhancement, and show the connection between far-field transmission and near-field intensity in a Fano model. Annular

#113798 - $15.00 USD Received 6 Jul 2009; revised 29 Jul 2009; accepted 30 Jul 2009; published 3 Aug 2009

aperture arrays that exhibit localized plasmon resonances also lead to upconversion enhancements, albeit of smaller magnitude. We experimentally demonstrate that the field enhancement due to the excitation of such modes is independent of incident angle.

We note that enhancing the strength of the upconversion process with plasmonic nanostructures is a valuable goal in itself. Upconversion is of importance in lasers [25–27], display technology [28], and luminescent probes in microscopy [29]. Moreover, it has been proposed as a possible route to enhance the efficiency of silicon solar cells. By converting part of the infrared solar radiation that is not captured by a silicon solar cell to radiation with shorter wavelengths, this part of the solar spectrum could be absorbed as well [30, 31]. However, all of these applications are hindered by the fact that the upconversion process is nonlinear in the excitation power and — in the case of rare earth ions — by the fact that typical absorption cross sections are small. Both facts limit the upconversion efficiency, especially at small pump powers. By making use of the enhanced fields of plasmonic resonances (which have large cross sections) as an intermediate step in the excitation of the emitters by incident light, their cross section can be effectively enhanced. This could lead to an increased upconversion efficiency [31–34], from which all of the above applications might benefit.

2. Methods

The aperture arrays are fabricated in a 110 nm thick Au film on a sapphire substrate. The substrate (refractive index 1.74) is first implanted with 200 keV Er^{+} ions at a fluence of 7×10^{15} cm^{-2} through a 10 nm thick Ge conducting layer, which is subsequently removed. This results in a Gaussian depth profile of implanted Er^{3+} ions at an average depth of 35 nm below the sapphire surface. The profile has a standard deviation of $\sigma = 12$ nm, as simulated with the Monte Carlo program SRIM [35]. The sample is annealed under an Ar atmosphere at 900 $^{\circ}$C for one hour to remove implantation related defects and activate the Er ions [36].

The arrays of holes in a Au film are fabricated by electron beam lithography and liftoff. The structures are patterned in a layered resist stack of 300 nm photoresist (S1813), 20 nm Ge and 100 nm negative electron beam resist (Ma-N 2401). The pattern is transferred to the layers underneath by reactive ion etching. The 110 nm thick Au film is evaporated directly on the substrate. The photoresist is finally stripped in a liftoff process. The size of each aperture array is 50×50 μm^2. Many arrays are fabricated, of which the period as well as aperture size and shape are varied. Two general aperture shapes are considered: square and annular (also termed coaxial). Figures 1(a,b) show SEM micrographs of details of both an array of square holes and an array of annular apertures. The annular apertures are designed to be square rather than circular, but these two types of hole shape are known to exhibit comparable behavior [37].

The measurement geometry is schematically depicted in Fig. 1(c). The arrays are illuminated from the air side of the Au film at normal incidence with a numerical aperture of 0.02, effectively illuminating individual arrays completely. The excitation source is a fiber-pigtailed 1480 nm CW diode pump laser (Fitel). To record broad-band transmission spectra, a fiber-coupled halogen lamp is used. Light from the sample is collected through the substrate using a microscope objective (NA=0.75), and focused on the entrance facet of a 100 μm core diameter optical fiber. Because the magnification of the microscope is 12.5×, only light originating from the center of the illumination spot is detected, and the illumination within this collection spot can therefore be considered as homogeneous. The collected Er upconversion emission or white light transmission is then led to a spectrograph and a Si CCD detector to record spectra for visible wavelengths, or to a spectrograph and a InGaAs photodiode array detector to record infrared transmission spectra.

For the angle-dependent measurements reported in section 5, the illumination optics are replaced by a microscope objective with an NA of 0.75. By limiting the width of the beam en-

#113798 - $15.00 USD Received 6 Jul 2009; revised 29 Jul 2009; accepted 30 Jul 2009; published 3 Aug 2009

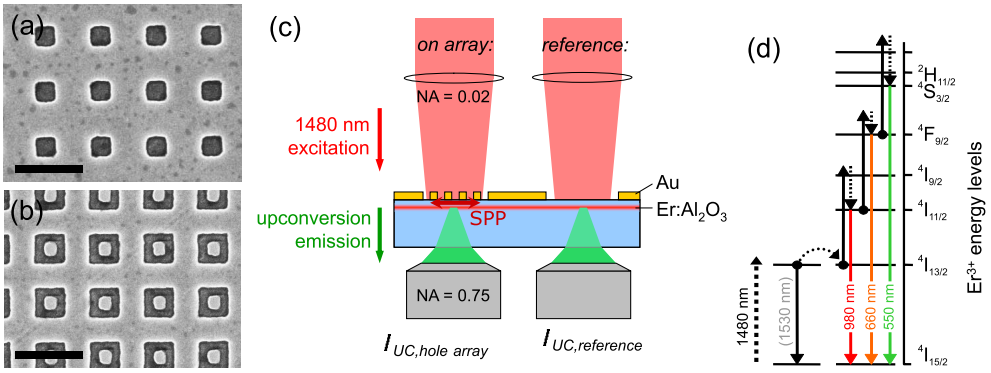

Fig. 1. (a) and (b) SEM micrographs of details of fabricated arrays of square and annular apertures, respectively. Scale bars are 1 μm. (c) Schematic depiction of the measurement geometry. The sample is illuminated with 1480 nm pump light, and upconversion luminescence from Er ions implanted in the sapphire substrate is collected through the substrate. (d) Er^{3+} $4f$ level diagram indicating the upconversion mechanism that leads to the population of Er^{3+} levels emitting at wavelengths of 980, 660, and 550 nm under 1480 nm excitation.

tering the back aperture of the objective, the illumination NA is effectively reduced to 0.1. The illumination angle is then controlled by displacing the beam that enters the objective with respect to the optical axis.

Upconversion emission from the Er ions is used as a probe of the local intensity of the 1480 nm excitation laser light. A level diagram of the $4f$ energy levels in Er^{3+} is shown in Fig. 1(d). The pump light excites Er ions to the first excited state, from which multiple upconversion processes can occur to populate higher Er levels [23, 24]. Two neighboring Er ions that are both excited can exchange energy in a dipole-dipole interaction to promote one to the $^4I_{9/2}$ level. The excited Er ion then quickly relaxes to the second excited state ($^4I_{11/2}$), which can emit a photon with a wavelength of 980 nm (see Fig. 1(d)). This process, based on Förster transfer between two excited Er ions, is called cooperative upconversion. A competing process is excited state absorption, in which a second pump photon is directly absorbed by an Er ion residing in the first excited state. Excited state absorption is especially strong for large incident fluxes. At small pump powers, both processes will result in a quadratic dependence of the 980 nm upconversion photoluminescence on the excitation power. However, at higher excitation powers the pump power dependence can deviate from this quadratic dependence due to saturation of the Er levels. Higher order upconversion processes can also populate Er levels emitting at wavelengths of 660 nm and 550 nm (see Fig. 1(d)), but in this work we will focus on the emission from the $^4I_{11/2}$ level at 980 nm. Because the emission wavelength is spectrally separated from the excitation wavelength, plasmon resonances will not simultaneously affect both excitation and emission channels. It is however impossible to exclude any effects on the upconversion emission due to the presence of the metal nanostructures, such as an altered branching ratio due to a changed local density of states at the emission wavelength [33] or emission into preferred directions due to grating diffraction. The effect of the latter is suppressed by collecting with a large numerical aperture. As we will show, it is possible to ascribe all observations in this paper to modifications of the Er excitation rate due to a variation in pump intensity in the near field of the aperture arrays.

The depth profile of Er ions is designed such that the ions do not directly quench to the Au film [38]. At a wavelength of 1480 nm, the intensity of SPPs on an uncorrugated Au/sapphire

#113798 - $15.00 USD Received 6 Jul 2009; revised 29 Jul 2009; accepted 30 Jul 2009; published 3 Aug 2009

interface decays into the substrate to $1/e$ of the maximum value within a distance of $\sim$390 nm. This means the intensity varies negligibly over the Er distribution. Nonetheless, near a corrugated film it is possible that the field varies within shorter length scales. We should consider the measured upconversion intensity therefore to be related to the field intensity averaged over the spatial distribution of the implanted Er ions.

3. Field enhancement in hole arrays: dependence on structural parameters

We first focus our attention to arrays of square-shaped holes. Figure 2 shows a white light transmission spectrum of an array with a periodicity of 810 nm and a hole diameter of 290 nm, normalized to the transmittance through the sample without the Au film. It shows three distinct transmission peaks for wavelengths longer than 800 nm. These maxima have been attributed to the excitation of surface plasmon polaritons that are excited when the condition

$$k_{SPP} = k_0 \sin\theta_0 + \frac{2\pi i}{a}\hat{x} + \frac{2\pi j}{a}\hat{y} \tag{1}$$

is satisfied [1, 39, 40]. Here k_0 and θ_0 are the free-space wavevector and angle of incidence, respectively. The array pitch is given by a. The integers i and j together specify the diffraction order (i, j) that couples to SPPs with wavevector k_{SPP}. It is important to note that k_{SPP} is a priori unknown, since it is an eigenmode of the corrugated surface (i.e. a pole of the scattering matrix of the array), and it depends on the exact geometry of the structure [12]. The two peaks with longest wavelengths correspond to excitation of the surface plasmon mode at the metal/sapphire surface, and they are therefore expected to enhance the field at the position of the Er ions.

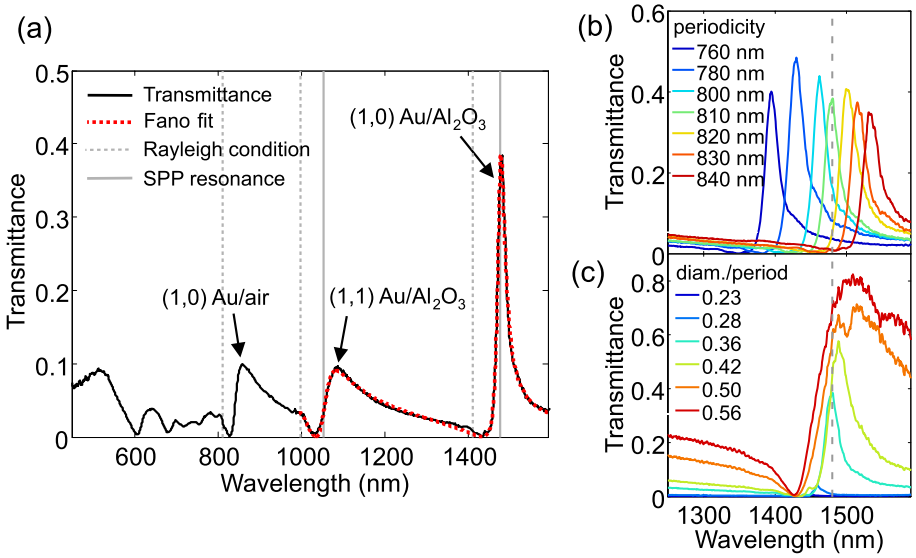

Fig. 2. (a) Transmission spectrum of a hole array in a Au film with a pitch of 810 nm. The red dotted curve is a fit of the Fano model described in section 4. The vertical gray lines indicate the resonance frequencies deduced from the Fano model, and the dashed gray lines depict the Rayleigh conditions for different diffraction orders. (b) Transmission spectra around the ($\pm$1,0) peak at the Au/Al_2O_3 interface for various array periods. (c) Evolution of the same transmission peak with increasing hole size (indicated as diameter/period.)

The resonance wavelengths can be precisely tuned by varying the array periodicity, as can be seen for the transmission peak associated to excitation of the surface wave at the Al_2O_3 inter-

#113798 - $15.00 USD Received 6 Jul 2009; revised 29 Jul 2009; accepted 30 Jul 2009; published 3 Aug 2009

face by the ($\pm$1,0) diffraction order in Fig. 2(b). The wavelength of the transmission maximum is a linear function of the periodicity to close approximation, since the SPP dispersion is nearly linear in this frequency regime. In the following experiment the periodicity is chosen such that the transmission peak coincides with the excitation wavelength of 1480 nm (see dashed line in Fig. 2(b)). This periodicity is 810 nm, as in Fig. 2(a). The upconversion photoluminescence spectrum as collected from that particular array is depicted by the red curve in Fig. 3, at an excitation power of 200 W/cm^2. Emission from four different Er manifolds that are all populated through upconversion processes is observed, at wavelengths of 550, 660, 810 and 980 nm. Also plotted is the luminescence spectrum obtained under equal experimental conditions in the absence of gold (through an aperture in the Au film of 50$\times$50 μm^2), multiplied by a factor 10. Clearly, the upconversion emission on the hole array is strongly enhanced with respect to that reference. In the following, we define the 'upconversion enhancement' caused by an array as the ratio of the collected upconversion photoluminescence intensity on that array and the detected upconversion emission in a reference measurement in the absence of the Au film.

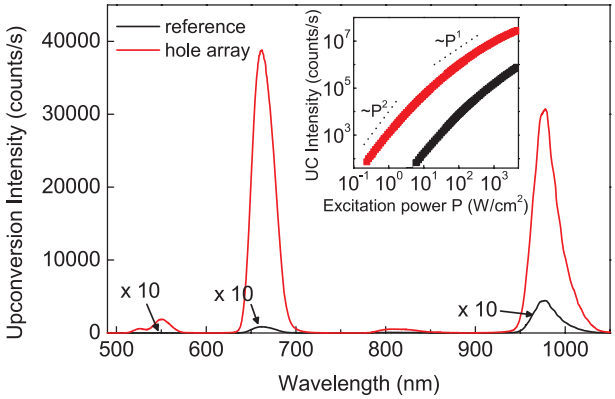

Fig. 3. Er upconversion spectra obtained from a hole array with a pitch of 810 nm (red) and from a reference in the absence of the Au film (black) under 1480 nm pumping at 200 W/cm^2. Spectral resolution is $\sim$20 nm. The inset depicts the dependence of the 980 nm emission on 1480 nm pump power, measured on the array (red) and on the reference (black).

We note that the measured upconversion enhancement does not directly reflect the average field enhancement at the position of the Er ions. The pump power dependence of the upconversion luminescence intensity is not a simple function such as a power law with a known exponent, which would make extraction of the pump power enhancement straightforward. The measured 980 nm upconversion emission as a function of 1480 nm pump power density is plotted on a double-logarithmic scale in the inset of Fig. 3, both on the array (red) and on the reference (black). For low pump powers, the upconversion luminescence can be seen to scale roughly quadratically with the excitation power as expected, but for larger pump powers saturation clearly occurs. By comparing the two curves, we can deduce a better estimate of the pump power enhancement on the array. We extract the pump powers for which the collected upconversion luminescence intensities on the array and on the reference are equal. The ratio of these pump powers represents the average field intensity enhancement at the position of the Er ions, since it tells us how much the pump intensity on the array can be diminished with respect to that of the reference, to still result in the same amount of emission. We find a field intensity enhancement of a factor 40. For practical reasons we will use the aforementioned upconversion enhancement to compare the field enhancement on different arrays. We note that the upcon-

#113798 - $15.00 USD Received 6 Jul 2009; revised 29 Jul 2009; accepted 30 Jul 2009; published 3 Aug 2009

version luminescence emitted at shorter wavelengths is even more strongly enhanced, as the corresponding Er levels are populated through higher order nonlinear upconversion processes. In the following, only the upconversion enhancement from the level emitting at a wavelength of 980 nm is considered.

We now systematically vary the periodicity and the hole diameter. Figure 4 shows the upconversion enhancement at an incident flux of 2 W/cm^2 as a function of array periodicity and hole size (expressed as the hole diameter divided by the period). By varying the period in this range, both the ($\pm$1,0) and the ($\pm$1,$\pm$1) transmission resonances corresponding to SPPs at the Au/sapphire interface can be tuned to the excitation wavelength, at periods of approximately 800 and 1150 nm, respectively (see arrows in Fig. 4).

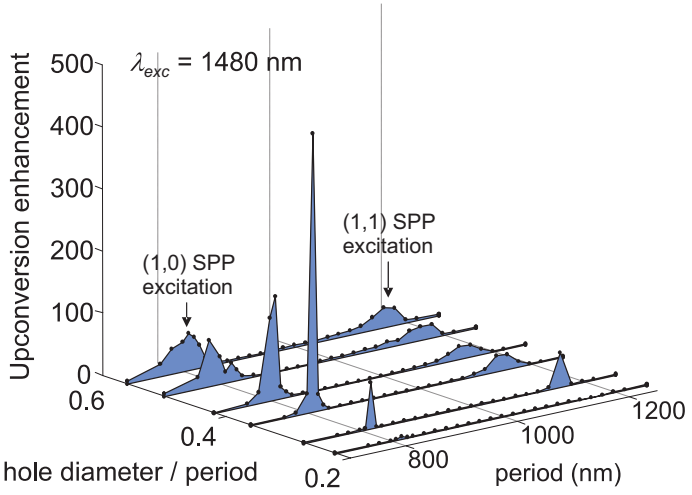

Fig. 4. 980 nm upconversion enhancement (under 1480 nm pumping at 2 W/cm^2) at an emission wavelength of 980 nm on hole arrays as a function of array period and hole size. Every point in the figure is derived from measurements such as in Fig. 3 on a corresponding array.

For a given enhancement peak, a strong dependence of the upconversion luminescence on the aperture size can be seen in Fig. 4. For the resonance excited with a period of $\sim$800 nm, maximum field enhancement is observed for a hole size that is 0.36 times the period, giving rise to a 450-fold upconversion enhancement. For larger holes, the field enhancement gradually decreases. Increasing the hole size will increase the evanescent tunneling of light through the holes as well as their scattering strength. Therefore the fraction of light coupled to SPPs will increase with increasing diameter. This becomes apparent as a monotonous increase of the far-field transmittance with increasing diameter [41], that is depicted in Fig. 2(c). The near-field enhancement represented by the data in Fig. 4 on the other hand reveals the existence of an optimum hole size. The stronger coupling between far-field radiation and SPPs for larger holes results in a widening and a redshift of the transmission peak. Both effects can be observed in the data in Fig. 4, as well as in the transmission spectra in Fig. 2(c). Unlike the far-field transmittance, the near-field enhancement does not only scale with the fraction of light coupled to SPPs, but also with the resonance linewidth. A larger quality factor of the SPP resonance results in a stronger build-up of optical energy close to the array. A trade-off therefore exists between quality factor and coupled fraction as the hole size is varied, resulting in an optimum hole size that yields maximum field enhancement. Note that this optimum strongly depends on other parameters as well; most notably the film thickness and the illumination geometry. If the array

#113798 - $15.00 USD Received 6 Jul 2009; revised 29 Jul 2009; accepted 30 Jul 2009; published 3 Aug 2009

would have been illuminated from the substrate side of the film, the exciting radiation would not have needed to tunnel through the apertures before exciting SPPs at the Au/sapphire interface, likely resulting in a stronger field enhancement at a smaller optimum hole size compared to the geometry studied here.

4. The Fano model: far field transmission and near field enhancement

We also investigate the relation between far-field transmittance and near-field enhancement by comparing their dependence on array periodicity. Figure 5 (red circles) shows the upconversion enhancement as a function of period for a hole diameter of 0.42 times the period from Fig. 4. Again, every data point represents a measurement on an array with a different periodicity. Also indicated is the transmittance at the excitation wavelength of 1480 nm on those same arrays. While both data sets show two maxima at similar periods (at 800 nm and ∼1150 nm), striking differences between the shapes of the curves can be observed. The transmission peaks are wider, shifted to smaller pitches (corresponding to a spectral redshift), and pronouncedly more asymmetric than the peaks observed in the near-field enhancement probed by the upconversion emission.

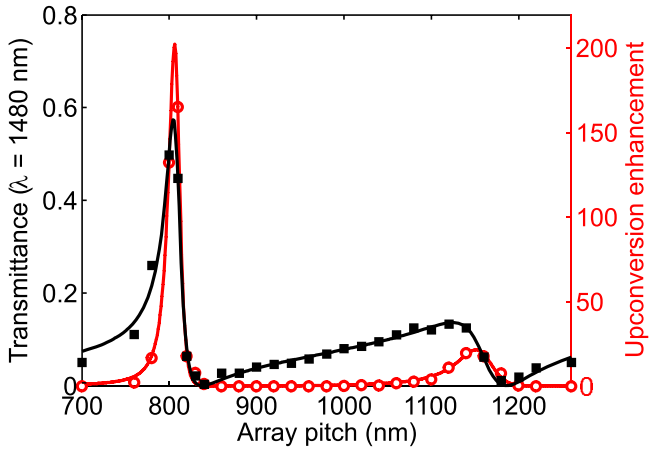

Fig. 5. Comparison between the 980 nm upconversion enhancement (red) and the transmittance at 1480 nm (black) as a function of the hole array period (hole diameter/period = 0.42). Each data point is measured on a different array. The curves are fits of a Fano model to the data. The resonance wavelengths and widths derived from the Fano model fitted to the transmittance data are imposed on the Fano model that is fitted to the upconversion enhancement data. The Fano model correctly predicts both the position and linewidth of the surface plasmon resonances, which are revealed by the upconversion enhancement.

These differences can be fully explained in terms of the Fano model [42]. The response of a subwavelength hole array can be described as that of multiple discrete states (the surface plasmon modes resonantly excited by various diffraction orders) coupled to a continuum (all far-field scattering states) [43, 44]. The array can scatter light to the far field either directly or by first exciting surface plasmons and subsequently radiating to the far field. These nonresonant and resonant channels can interfere to produce asymmetric transmission spectra when both contributions are of approximately equal magnitude, as the resonant channel acquires an opposite phase as the frequency crosses the resonance [42]. The spectral shape, generalized to a

#113798 - $15.00 USD Received 6 Jul 2009; revised 29 Jul 2009; accepted 30 Jul 2009; published 3 Aug 2009

system of multiple resonances with resonance frequencies ω_r and linewidths γ_r is given by [17]

$$T(\omega) = T_a \frac{\left(1+\sum_r q_r/\varepsilon_r\right)^2}{1+\left(\sum_r \varepsilon_r^{-1}\right)^2}, \quad \text{with} \quad \varepsilon_r = \frac{\omega-\omega_r}{\gamma_r/2}, \tag{2}$$

where T_a is a slowly varying background representing the non-resonant transmission channel and q_r is a shape parameter that is related to the strength and phase of the resonant channel with respect to the non-resonant contribution. To illustrate the potential of this model we return to the transmission spectrum of the hole array with a pitch of 810 nm shown in Fig. 2. We fit Eq. 2 to this spectrum for wavelengths larger than 1000 nm, allowing for two resonances. The non-resonant contribution T_a is assumed to scale as λ^{-4}, in accordance with the transmittance of a circular aperture of a perfectly conducting screen as given by Bethe [45]. The excellent fit of the Fano model (the red dashed line in Fig. 2) to the experimental transmission spectrum suggests that the most important physics of the system is indeed determined by the two surface wave resonances. The transmission peaks are redshifted with respect to the fitted resonance frequencies, which are indicated by the grey lines. For comparison, the Rayleigh conditions, for which the right-hand side of Eq. 1 equals the wavevector of light in the bounding dielectrics, are indicated by the grey dashed lines. As an aside, we note that the peak associated with ($\pm$1,0) diffraction to surface plasmons at the Au/air interface can also be fitted when a third resonance is introduced. However, in that case it becomes apparent that the assumption $T_a \propto \lambda^{-4}$ overestimates the direct transmission through the apertures at small wavelengths. A better fit is obtained for $T_a \propto \lambda^{-3}$. An explanation for a deviation from Bethe's theory could be sought in the finite thickness of the metal film and metal absorption.

While the above analysis regards measurements of the far-field transmission, the Fano effect can play a role in the near-field as well, because the field of the resonantly excited surface plasmons can interfere with the incident field transmitted through the apertures. But because the surface plasmon field is strongly enhanced (by a factor related to the resonance linewidth), the shape parameter q will in general be much larger, making the resonant contribution dominant. This is reflected in the differences between the transmittance and upconversion enhancement data sets for varying periodicity in Fig. 5. We first fit the Fano model (Eq. 2) to the transmittance data in Fig. 5, where ω is fixed by the laser wavelength and we assume that the resonance frequencies ω_r are inversely proportional to the periodicity a: $\omega_r = c_r a^{-1}$ (the SPP dispersion is nearly linear near 1480 nm). We again assume that the direct transmission through a single hole scales as $(\lambda/R)^{-4}$. The hole radius R scales linearly with the period a. Because the hole density decreases quadratically with increasing period and the wavelength λ is fixed, we now have to take $T_a \propto a^2$. An excellent fit to the transmittance data is obtained, depicted by the black curve in Fig. 5. We then fit the upconversion enhancement data by taking the values for c_r and γ_r derived from the fit of the transmittance data, only fitting q_r and T_a. The fit resulting from this procedure is depicted as the red line in Fig. 5. In the analysis the measured power-dependence (see the inset of Fig. 3) has been taken into account to yield the upconversion enhancement from the field intensity enhancement given by the Fano model. A near-perfect fit to the data is obtained. The larger relative contribution of the resonant channel to the near field results in almost Lorentzian lineshapes of the resonances observed in the upconversion enhancement, centered around the resonant periodicity. The transmission maxima are significantly shifted and broadened with respect to the actual surface wave resonance, as is most clear for the peak at a pitch of $\sim$1150 nm (for which the hole size and therefore the nonresonant contribution are largest). Similar shifts were reported for second harmonic generation in aperture arrays [8, 10, 11]. The Fano interpretation presented here yields a new and powerful explanation for those observations. These results show that the Fano model correctly predicts the wavelength and

#113798 - $15.00 USD Received 6 Jul 2009; revised 29 Jul 2009; accepted 30 Jul 2009; published 3 Aug 2009

spectral width of the surface plasmon eigenmodes of the corrugated surface. The luminescence from emitters placed in the near field of hole arrays can be used to experimentally reveal the surface modes that are responsible for the extraordinary transmission phenomenon [1, 12, 40].

5. Field enhancement in arrays of annular apertures: propagating and localized resonances

The field enhancement in arrays of round or square subwavelength holes depends strongly on the frequency and the angle of incidence, as it relies to a large degree on grating diffraction (see Eq. 1). In contrast, field enhancement due to localized resonances such as those supported by annular apertures does not suffer from this limitation. The transmission spectra of arrays of annular apertures can exhibit features that are due to the excitation of both localized and propagating modes [17, 19]. Figure 6(a) shows the transmission spectra of annular aperture arrays in Au consisting of apertures of varying size. The array period is kept constant at 800 nm. We denote the length of the side of the Au island as D_1 and the length of the side of the total aperture as D_2 (see inset in Fig. 6(b)). Both D_1 and D_2 are continuously increased, starting from array A (dark blue) to array C (dark red). Due to fabrication intricacies, it was not possible to keep the ratio of D_1 to D_2 perfectly constant throughout the series. Therefore, we include SEM micrographs of three of the annular aperture shapes in the legend of Fig. 6. The transmission spectrum of array A shows a strong resemblance to that of an array of square holes in the absence of the central Au island (black), displaying the diffractive resonances described in the previous sections. As the aperture size increases, the transmission peaks broaden and increase in magnitude, until for the largest apertures (array C) a single broad transmission peak dominates the spectrum for wavelengths larger than 1100 nm, which we attribute to a localized resonance. These aperture dimensions agree roughly to the cutoff condition of the TE_{11} mode in a perfectly conducting waveguide [20], which scales to first order with $(D_1 + D_2)$. Note that grating effects observed for the regular holes such as the minimum around 1400 nm are in this case largely suppressed.

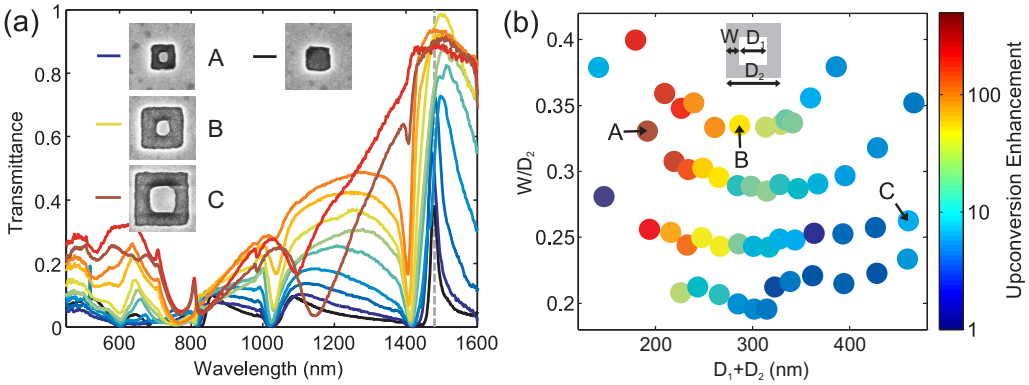

Fig. 6. (a) Transmission spectra of annular aperture arrays for increasing aperture size (array period 800 nm). The black curve is the transmittance of an array of square holes with the same period. (b) 980 nm upconversion enhancement (1480 nm pump at 2 W/cm^2) as a function of the main parameters describing the shape of the annular apertures: the sum of D_1 and D_2, and the width of the air gap W expressed as a fraction of the total aperture size D_2.

In Fig. 6(b) we plot the measured upconversion enhancement on a collection of arrays with varying aperture dimensions. The horizontal axis specifies the sum of D_1 and D_2 of the an-

#113798 - $15.00 USD Received 6 Jul 2009; revised 29 Jul 2009; accepted 30 Jul 2009; published 3 Aug 2009

nular apertures, and the vertical axis denotes the width of the air gap between the central Au island and the continuous Au film W, expressed as a fraction of the total aperture size D_2. The periodicity of all arrays is 800 nm, and the excitation power is 2 W/cm^2. The overall trend in Fig. 6(b) is that largest upconversion enhancements are observed for the smaller radii. Enhancements of over a factor 100 are observed for radii around 100 nm. The maximum upconversion enhancement factor is achieved on array A, which exhibits a transmission maximum related to the excitation of propagating surface plasmons that is resonant with the 1480 nm excitation wavelength. The magnitude of the enhancement is a factor 370, comparable to the maximum enhancement observed on arrays of square holes. Array C, which supports a localized resonance (see Fig. 6(a)), yields a lower enhancement factor of approximately 10. Nonetheless, the field enhancement in this structure is larger than in structures with slightly different gap widths or sizes, which we attribute to the enhanced spectral overlap of the corresponding localized resonance to the excitation wavelength for this aperture shape.

Finally, we investigate the effect of the angle of incidence on the field enhancement due to either propagating or localized resonances. Figure 7 shows the measured upconversion enhancement on three different aperture arrays as a function of angle of incidence as described in section 2. The incident light is *p*-polarized. As expected, the upconversion enhancement on array A, which is associated to the excitation of propagating SPPs, shows a strong dependence on the incident angle, vanishing for angles larger than 10°. Note that the maximum enhancement at normal incidence is now reduced compared to that in Fig. 6(b) due to the use of a larger NA. The maximum enhancement on array B is observed for an incident angle of $\sim 6°$. For this array, the resonance was not tuned exactly to the laser wavelength at normal incidence. Instead, Eq. 1 is satisfied at a slightly different angle. The upconversion enhancement diminishes less rapidly for larger angles than for array A, since the resonance width is larger in this case. Nonetheless, still a clear angle-dependence is observed. Array C does not show an effect of the incident angle on the upconversion enhancement, which is $\sim$10 for the angular range studied here. This shows that the field enhancement due to localized plasmonic resonances in annular aperture arrays is indeed independent on the incident angle.

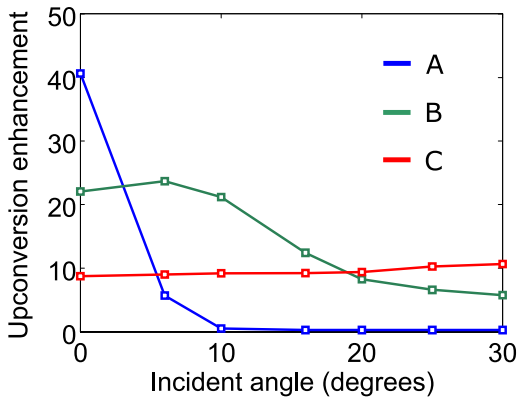

Fig. 7. 980 nm upconversion enhancement as a function of incident angle for three different annular aperture arrays specified in Fig. 6 (1480 nm pump at 16 W/cm^2). The field enhancement that is caused by a localized resonance (array C) is independent of the angle of incidence.

#113798 - $15.00 USD Received 6 Jul 2009; revised 29 Jul 2009; accepted 30 Jul 2009; published 3 Aug 2009

6. Conclusions

We have shown that Er upconversion luminescence can be used to probe the field enhancement in subwavelength aperture arrays. Field enhancement due to the excitation of both propagating and localized resonances in aperture arrays was studied. In hole arrays supporting propagating resonances, an enhancement of the 980 nm upconversion luminescence of Er ions under 1480 nm pumping by a factor 450 is demonstrated. This maximum upconversion enhancement is achieved for a hole size that balances SPP coupling efficiency and resonance linewidth. We note that the field enhancement can be further increased by changing the experimental geometry. The evanescent tunneling of the excitation light incident from the air side of the sample to excite SPPs at the substrate side of the sample (where the Er ions are located) limits the measured upconversion enhancement in the present geometry.

We confirm that the Fano model accurately predicts the frequencies and linewidths of the resonances that cause the extraordinary transmission phenomena. These properties are revealed by observing the Er upconversion enhancement. The relative strength of the resonant contribution to the near-field enhancement with respect to the non-resonant contribution is much larger than the ratio of both contributions in far-field transmission spectra. This results in much more symmetric lineshapes of the upconversion enhancement. The transmission peaks are significantly redshifted from the spectral position of maximal field enhancement.

We demonstrate that the transmission spectra of annular aperture arrays can be tuned by varying the aperture size, from an array exhibiting propagating surface plasmon resonances to one that supports localized plasmon resonance in the individual apertures. While the field enhancement is smaller in the latter case, we show experimentally that, unlike the field enhancement related to the excitation of propagating SPPs, this enhancement is independent of the angle of incidence.

This work reveals basic mechanisms governing near-field enhancement in metallic subwavelength aperture arrays, which is important for many practical applications of such nanostructures. In doing so, it sheds light on the mechanisms behind far-field extraordinary transmission properties as well.

Acknowledgements

This work was made possible by the fabrication and characterization facilities of the Amsterdam nanoCenter. It is part of the Joint Solar Programme (JSP) of the Stichting voor Fundamenteel Onderzoek der Materie (FOM), which is financially supported by the Nederlandse organisatie voor Wetenschappelijk Onderzoek (NWO). The JSP is co-financed by gebied Chemische Wetenschappen of NWO and Stichting Shell Research.

#113798 - $15.00 USD Received 6 Jul 2009; revised 29 Jul 2009; accepted 30 Jul 2009; published 3 Aug 2009